Title: Synapses are uniquely vulnerable to sleep loss during brain development while maturation confers resilience

Authors: Sean M. Gay[1], Elissavet Chartampila[1], Julia S. Lord[1], Sawyer Grizzard[1], Tekla Maisashvili[1], Michael Ye[1], Natalie K. Barker[2], Angie L. Mordant[2], C. Allie Mills[2], Laura E. Herring[2], Graham H. Diering[1,3,4]*

Affiliations:

[1]Department of Cell Biology and Physiology, University of North Carolina at Chapel Hill; Chapel Hill, NC, USA.

[2]UNC Proteomics Core Facility, Department of Pharmacology, University of North Carolina at Chapel Hill; Chapel Hill, NC, USA.

[3]Neuroscience Center, University of North Carolina at Chapel Hill; Chapel Hill, NC, USA.

[4]Carolina Institute for Developmental Disabilities; Chapel Hill, NC, USA.

*Corresponding author. Email: graham_diering@med.unc.edu

Abstract: Sleep supports lifelong brain health and cognition. Sleep loss in early life can drive lasting changes in adult behavior, indicating sleep plays a distinct but poorly understood role in brain development. We systematically examined the homeostatic adaptations and synaptic consequences of acute sleep deprivation (SD) in developing and adult mice. Developing mice lack robust homeostatic adaptations to SD, exacerbating cognitive deficits. Synapse proteome and phosphoproteome analysis revealed profound vulnerability to SD in developing mice, including immediate impacts on synaptogenesis and key aspects of brain development. With maturation, a unified biochemical effect of sleep on synapses emerges, together with robust homeostatic adaptations and resilience to SD. Our findings show sleep plays a distinct role in early life supporting synapse development, transitioning to homeostatic functions with maturation.

One-Sentence Summary: Effects of sleep loss across life stages indicate sleep plays a distinct role in early life supporting synapse maturation.

Main Text:

Sleep is a lifelong, essential, and conserved process that supports health and cognition. While the behavioral switching between wake/sleep states is controlled by discrete neuronal populations, the need for sleep is broadly expressed across the brain and accumulates in a homeostatic manner with time spent awake, most notably in excitatory neurons (*1, 2*). Neuronal synapses of the mammalian forebrain undergo widespread modifications during sleep and accumulate protein phosphorylation downstream of sleep-promoting kinases in response to sleep deprivation (SD) (*3-6*). Thus, synapses are both a locus for accumulation of sleep need and a target of restorative sleep function. Sleep behavior, and synapse density are highly dynamic during postnatal development (*7, 8*), leading to a critical unanswered question: does sleep perform the same beneficial function throughout the lifespan? Importantly, sleep disruption during sensitive periods of development is causal in long-lasting changes in behavior in numerous species (*9-11*), leading to the clear hypothesis that sleep performs unique functions in early life supporting brain development. This idea is supported by recent mathematical modeling concluding that sleep, across species, plays a completely distinct role during early development supporting brain growth, transitioning to homeostatic functions with maturation (*12*).

To test this idea, and to identify nodes of vulnerability to sleep loss in the developing brain, we systematically analyzed the molecular and behavioral effects of acute 4-6hr SD (SD4/6), starting from lights on (ZT0) in wild-type juvenile (postnatal day P21-28), adolescent (P42-45), and adult (P90-100) mice, including both sexes. Adult mammals respond to SD through behavioral, physiological, and molecular homeostatic adaptations. SD induces sleep rebound behavior, an increase in subsequent sleep amount during recovery, and increased non-rapid eye movement sleep slow-wave activity (NREM-SWA) measured by electroencephalography (EEG) (*1, 13-15*). At the molecular level SD drives broad induction of immediate early gene and homeostatic scaling factor *Homer1a (14-16)*, referred to as “the molecular marker of sleep need”. Surprisingly, whether these well characterized homeostatic adaptations to SD in adults are differentially expressed during development is not well described.

Developing mice lack robust homeostatic adaptations to sleep deprivation seen in adults

Using non-invasive home-cage sleep recording, we systematically measured sleep rebound behavior in response to acute 4hr SD (SD4) in developing and adult mice. As expected (*14, 15*), adults showed a significant increase in dark phase sleep following SD4 in comparison to the preceding baseline day, a clear demonstration of sleep rebound behavior. Strikingly, dark phase sleep rebound was completely absent in juveniles and severely blunted in adolescents (Fig. 1A-C). Consequently, adult mice were able to recover the majority of sleep loss within 24hrs, whereas developing mice retained the majority of accumulated sleep debt (Fig. 1D). Next, we measured forebrain transcripts of homeostatic scaling factor *Homer1a* and circadian clock component *Per2* in undisturbed mice 4hrs into the sleep phase (S4/ZT4), wake phase (W4/ZT16), or immediately following SD4 (ZT4). As expected (*16*), compared to sleep, SD4 in adults resulted in robust induction of synaptic scaling factor *Homer1a*, a response that was also completely absent in juvenile mice, and severely blunted in adolescents. In contrast, comparable SD-induction of *Per2* was observed in all three ages (Fig. 1E). *Homer1a* is a driver of synapse remodeling during sleep in adults (*3*). This finding suggests that circadian adaptations to sleep loss are intact by the juvenile age, whereas homeostatic synaptic adaptations are not, further suggesting that the developing synapse may be uniquely vulnerable to sleep loss. A previous systematic EEG analysis of the effects of SD across development reported that the well

characterized SD-induced increase in NREM-SWA above baseline was also absent in juvenile mice and does not become apparent until mice reach ~P42 (*13*) (age referred to here as adolescence). Together, the complete absence of well characterized behavioral, physiological, and molecular homeostatic adaptations to sleep loss may expose juvenile mice to greater negative consequences of SD, negatively affecting cognition and brain maturation. Emergence of such adaptations during maturation may confer resilience to the negative consequences of SD. Accordingly, memory performance in the novel object recognition (NOR) task was completely impaired in juvenile mice treated by SD4 immediately following training in comparison to undisturbed controls (Fig. 1F, G, and fig. S1). In contrast, memory performance in adolescents and adults was resilient to SD4; extended SD6 impaired memory performance in adults (Fig. 1G). These findings clearly demonstrate that juvenile mice display heightened vulnerability to the negative consequences of SD compared to older mice, consistent with the emergence of adaptive responses to SD with maturation.

The synapse proteome of juvenile, adolescent, and adult mice are distinctly affected by SD

To identify synaptic mechanisms underlying developmental vulnerability and adult resilience to SD, we measured the immediate effects of SD on the developing and adult forebrain synapse proteome (Fig. 2) and phosphoproteome (Fig. 3), using subcellular fractionation and tandem-mass-tag (TMT) quantitative mass spectrometry. Mice were maintained on a 12:12hr light/dark cycle. Juveniles and adolescents were sacrificed undisturbed during the sleep phase (S4; ZT4), wake phase (W4; ZT16), or immediately following SD4 (ZT4); adults were sacrificed immediately following SD6 (ZT18) with matching undisturbed sleep (S6/ZT6) and wake conditions (W6/ZT18). We then isolated the forebrain synapse fraction, commonly referred to as the "post-synaptic density" (PSD) for analysis (Fig. 2A and B)(*3*). We identified and quantified ~5,000 proteins in forebrain synapse fractions from each age. Importantly, the majority of synapse proteins detected (4,391) were identified in all three ages (Fig. 2C), suggesting that we are able to reasonably compare the synaptic response to SD across the ages tested here.

By performing pairwise comparisons between wake/sleep/SD conditions, our experimental design allows for identification of synapse proteins regulated by the circadian rhythm (time of day), sleep-wake vigilance states, a selective response to SD, or a combination, in developing and adult mice, independent of sex (Fig. 2D and fig. S2). We first identified significantly regulated synapse proteins/phosphopeptides: ($p<0.05$) in one or more pairwise comparisons between conditions, followed by assignment to regulation groups: sleep/wake cycle, circadian rhythm, sleep deprivation, combined, or ambiguous (described in fig. S2). Note, biochemical analysis on bulk tissue is well suited to identify a unified, net effect of experimental conditions. In the juvenile W4/S4 comparison, we observed 55 significantly altered proteins, representing only 0.9% of the synapse proteome, consistent with reports that mixed types of plasticity co-occur during sleep at the juvenile age, including synapse strengthening and weakening/pruning (*17, 18*). In contrast, SD4/S4 and SD4/W4 comparisons showed 768 (13.0%) and 842 (14.3%) significantly altered proteins respectively (Fig. 2E), clearly indicating that SD drove a very large unified biochemical effect on juvenile synapses readily detected by our analysis. Overall analysis of juveniles showed 1,152 proteins (19.5% of the total synapse proteome) significantly altered between the three conditions, of these a clear majority, 62% showed a selective response to SD (Fig. 2H), compared to only ~2% each for circadian rhythm or wake-sleep cycle, indicating the developing synapse proteome is profoundly sensitive to SD.

A dramatic transition in synaptic responses occurs with maturation to adolescence and adulthood. Compared to the minimal W4/S4 changes seen in juvenile, we observe the emergence of a unified change between wake and sleep conditions where the W4/S4 comparison in adolescents revealed 351 (7.2%) proteins, and W6/S6 comparison in adults revealed 629 (9.5%) altered proteins (Fig. 2F and G). Overall, in adolescents we identified 796 (16.4%) regulated proteins between conditions. Interestingly, compared to juveniles, adolescents display a comparable reduction in the fraction of regulated proteins responding selectively to SD (22%), and emergence of a considerable component (34%) regulated by the circadian rhythm, with only 3% selectively responding to wake-sleep cycle (Fig. 2I). Finally, in adults we identified 772 (11.7%) regulated proteins, of these the clear majority (68%) were regulated as a function of the wake-sleep cycle, with only 2-3% of proteins selectively responding to SD or circadian rhythm (Fig. 2J). Indeed, the SD6/W6 comparison in adults, where both conditions are awake but at opposite times of day, showed almost no differences. This latter point is entirely consistent with recent multi-omics studies examining the daily regulation of the adult forebrain synapse, reporting that the synaptic translatome (synapse localized mRNA) is regulated primarily as a function of the circadian rhythm, whereas the synaptic proteome and phosphoproteome are regulated almost exclusively as a function of wake-sleep states (*4*, *5*). Consistent with adult resilience to SD4 in the NOR test (Fig. 1G), we find that SD4 treatment has a minimal effect on the adult synapse proteome compared to SD6 (Fig. S3A). Finally, comparison of significantly regulated proteins across ages and conditions revealed minimal overlap, indicating an almost entirely distinct proteomic response at each age, particularly notable for the juveniles (Fig. 2K-M). One exception was proteins upregulated in the wake/sleep comparison in adolescents and adults, which showed 148 shared proteins (Fig. 2K). This suggests a unified biochemical effect of wake/sleep conditions on synapses emerges with maturation past the juvenile period, as predicted by modeling (*12*).

SD drives a predominant phosphorylation-based response after maturation to adolescence

Next, we examined the dynamics of the synaptic phosphoproteome in juveniles, adolescents and adults. Previous phosphoproteomics studies revealed that the adult synapse phosphoproteome is regulated primarily as a function of the wake sleep cycle (*5*) and that SD drives accumulation of brain wide protein phosphorylation, primarily on synaptic proteins (*6*). Results of our analysis corroborate these prior findings from adults, but further indicate that the developing synapse phosphoproteome shows an entirely distinct SD response. Between comparisons we identified 1,790 regulated synaptic phosphopeptides from juveniles, representing 11.7% of the phosphoproteome, a majority of which showed a selective response to SD compared to only 5% responding to circadian rhythm (Fig. 3A and D). In adolescents we observed striking dynamics of the phosphoproteome in each comparison, far greater in magnitude than the other age groups. In total, 5,285 phosphopeptides (33.4%) were found to be significantly regulated, a large fraction of which (46%) showed a selective response to SD, and 13% were regulated by the circadian rhythm (Fig. 3B and E). In adults, SD6/W6/S6 analysis revealed 1,845 regulated phosphopeptides (11.4%), of which a majority (51%) showed a selective response to wake-sleep cycle, and only 7% showed a selective response to SD (Fig. 3C and F), consistent with prior literature (*5*). Substantially fewer phosphorylation changes, 2.6% of the phosphoproteome, were observed in the adults SD4/W4/S4 analysis (fig. S3B), consistent with a time of SD “dose response” of the phosphoproteome (*6*). In agreement with conclusions from the synapse proteome analysis (Fig. 2), regulated phosphopeptides showed minimal overlap between ages and conditions, indicative of a distinct phosphorylation response to SD at each age

(Fig. 3G-I). Accordingly, kinase substrate enrichment analysis (KSEA), which predicts kinase activity based phosphorylation data (*19*), suggests distinct patterns of kinase activation between ages (Fig. S4),

Consistent with prior literature (*6*), SD drove an asymmetric accumulation of phosphorylation in the SD/sleep comparison for adolescents and adults (Fig. 3B and C). Interestingly, this pattern was not observed in juveniles, which showed slightly more decreased phosphorylations (Fig. 3A). We additionally examined phosphorylation changes occurring on previously identified "sleep-need index phosphoproteins" (SNIPPs), mostly synaptic localized proteins demonstrated to preferentially accumulate phosphorylations in response to SD (*6*). Compared to sleep, SD drove an asymmetric increase in SNIPP phosphorylation in adolescents and adults, whereas juvenile mice displayed a largely symmetrical change in SNIPP phosphorylation (fig. S5). This is indicative of a molecularly distinct SD response in juveniles, and emergence of a phosphorylation-based response with maturation through adolescence. Notably, the synaptic phosphorylation response in adolescents was substantially greater compared to adults, affecting more than twice the number of phosphopeptides (Fig. 3B and E). Previous phosphoproteomic analysis indicated synapse phosphorylation accumulates in response to duration, "dosing", of SD (*6*). We speculate that blunted homeostatic sleep rebound and *Homer1a* responses to SD in adolescents compared to adults (Fig. 1) may minimize the ability of adolescents to mitigate sleep need accumulation, leading to acceleration of the synaptic phosphorylation response downstream of sleep promoting kinases (*2, 20-22*).

Sleep deprivation in juveniles drives immediate impacts on key aspects of brain development

Recent mathematical modeling examining sleep across life stages and species predicted a unique developmental function of sleep in early life supporting brain growth, abruptly transitioning to a homeostatic function with maturation (*12*). Differential sleep function further predicts SD will drive distinct consequences across development. Accordingly, gene ontology (GO) and STRING pathway analysis of SD sensitive proteins revealed that SD in juveniles, but not adolescents or adults, drove upregulation of dozens of synaptic proteins related to axon-growth, synaptogenesis, myelination, and formation of perineuronal nets (PNNs) (Fig. 4A). These pathways represent key aspects of brain development actively shaping neuronal networks during the juvenile period (*23-28*). In addition, SD in juveniles but not older groups drove upregulation of synapse proteins related to excitatory synaptic strengthening and Hebbian LTP, including DLG4 (PSD95) and prominent excitatory synapse scaffolds, CaMKIIα, AMPA and NMDA-type glutamate receptors and auxiliary subunits (Fig. 4A)(*29, 30*). This suggests that SD in juveniles drives heightened neuronal activity that aberrantly stimulates synapse growth and potentiation. Consistent with this interpretation, kinase activity prediction indicates the SD in juveniles drives activation of CaMKIIα/β/γ (Fig. 4B and fig. S4), Ca^{++} activated kinases well known for a prominent function in Hebbian LTP (*30*). This is distinct from the predicted SD induced activation of PKCα/β/γ in adolescents (Fig. 4B and fig. S4).

During the juvenile period examined, the brain is still growing, having reached 70-80% of the final adult volume. Immediate sensitivity of synaptogenesis, axon-pathfinding, and formation of extracellular matrix to SD informs possible mechanisms to explain how early life sleep disruption can drive permanent effects on adult behavior (*9-11*). Sleep disruption is a common and early phenotype associated with autism spectrum disorder (ASD), an early onset

neurodevelopmental condition largely regarded as a synaptopathy (*31*). Moreover, sleep disruption is proposed to be a driver of behavioral and brain growth phenotypes in ASD (*32-35*). Importantly, we observed that proteins upregulated in response to SD in juveniles are significantly enriched for high-confidence ASD risk genes compiled by SFARI (Simons Foundation Autism Research Initiative, Fig. 4C and D). Adolescents showed a distinct pattern of enrichment of SFARI genes encoding proteins downregulated in response to SD (Fig. 4E and F). These findings suggests that developmental vulnerability to SD converges on nodes of genetic risk for neurodevelopmental disorders, acting synergistically to drive altered brain development and behavior in an age specific manner, as we have recently demonstrated (*11*).

With maturation, we observed emergence of resilience to SD and a net biochemical effect in wake/sleep comparisons from adolescents and adults (Fig. 2G, I, K), consistent with an abrupt transition in sleep function predicted by mathematical modeling (*12*). Compared to sleep, adolescents and adults showed an upregulation during wake of numerous signaling and biochemical pathways including classic protein kinase C isoforms (PKCα/β/γ), as well as proteins related to phosphoinositide, Ras/MAPK, and Ca^{++}-activated signaling, ubiquitin and small GTPase cycle, and neuronal cilia (Fig. 4G). In adults, these proteins are almost entirely regulated as a function of wake sleep states, whereas in adolescents these proteins show a more complex pattern including circadian rhythm (Fig. 2I). This raises the intriguing possibility that the circadian rhythm plays a critical step in maturation towards the ultimate regulation of the adult synapse by wake/sleep states (*4, 5*). Together, our behavioral, molecular, proteomic, and phosphoproteomic analyses (Fig. 1-3) all clearly indicate distinct responses to SD between juvenile, adolescent, and adult mice, indicative of unique functions of sleep across development (Fig. 4H).

Discussion

Sleep is a lifelong, essential process shared across animal evolution. Despite abundant evidence that neuronal synapses are one major target of restorative sleep function, the mechanism(s) of beneficial synaptic modifications has been a topic of considerable controversy. Contrasting findings reported in the literature between developing and adult subjects may be a major source of this controversy (*3, 7, 36-38*). Recent mathematical modeling (*12*) and our current findings strongly indicate that sleep plays a unique role in shaping brain/synapse development in early life, transitioning to homeostatic functions with maturation. Distinct responses to SD between juvenile and adult mice is also supported by recently reported RNAseq analysis (*39*). The majority of neuronal synapses in the forebrain are formed after birth, during a period of profound synaptogenesis, followed by a period of activity dependent synapse pruning before synapse densities finally stabilize during maturation to adulthood (Fig. 4H)(*8*). During the juvenile period sleep has been demonstrated to be critical for the selection of synapses to be pruned and for the maturation and growth of the surviving synapses (*17, 40-42*). With maturation to adolescence and adulthood, when synapse densities stabilize, sleep drives a broad weakening and shrinkage of synapses through homeostatic scaling-down (*3, 43*), offsetting synaptic potentiation driven by information encoding during wake (*1*). Sleep disruption is associated with many neurological and neuropsychiatric illnesses across the lifespan. Our findings provide mechanistic insights into how sleep disruption in early life contributes to ASD, a relatively common neurodevelopmental disorder. With maturation to adulthood, the expression of robust homeostatic adaptations confers resilience to the negative consequences of SD. Waning of adult

resilience with aging may again expose the brain to heightened vulnerability to SD, contributing to age related cognitive decline and neurodegeneration (*44-46*). Recognition that sleep performs distinct functions across the lifespan will enable further advances in understanding the molecular basis of restorative sleep function, and the role of sleep in lifelong health and cognition.

References and Notes

1. G. Tononi, C. Cirelli, Sleep and the price of plasticity: from synaptic and cellular homeostasis to memory consolidation and integration. *Neuron* **81**, 12-34 (2014).
2. S. J. Kim *et al.*, Kinase signalling in excitatory neurons regulates sleep quantity and depth. *Nature* **612**, 512-518 (2022).
3. G. H. Diering *et al.*, Homer1a drives homeostatic scaling-down of excitatory synapses during sleep. *Science* **355**, 511-515 (2017).
4. S. B. Noya *et al.*, The forebrain synaptic transcriptome is organized by clocks but its proteome is driven by sleep. *Science* **366**, (2019).
5. F. Bruning *et al.*, Sleep-wake cycles drive daily dynamics of synaptic phosphorylation. *Science* **366**, (2019).
6. Z. Wang *et al.*, Quantitative phosphoproteomic analysis of the molecular substrates of sleep need. *Nature* **558**, 435-439 (2018).
7. M. G. Frank, The Ontogenesis of Mammalian Sleep: Form and Function. *Curr Sleep Med Rep* **6**, 267-279 (2020).
8. P. Penzes, M. E. Cahill, K. A. Jones, J. E. VanLeeuwen, K. M. Woolfrey, Dendritic spine pathology in neuropsychiatric disorders. *Nat Neurosci* **14**, 285-293 (2011).
9. M. S. Kayser, Z. Yue, A. Sehgal, A critical period of sleep for development of courtship circuitry and behavior in Drosophila. *Science* **344**, 269-274 (2014).
10. C. E. Jones *et al.*, Early-life sleep disruption increases parvalbumin in primary somatosensory cortex and impairs social bonding in prairie voles. *Sci Adv* **5**, eaav5188 (2019).
11. J. S. Lord *et al.*, Early life sleep disruption potentiates lasting sex-specific changes in behavior in genetically vulnerable Shank3 heterozygous autism model mice. *Mol Autism* **13**, 35 (2022).
12. J. Cao, A. B. Herman, G. B. West, G. Poe, V. M. Savage, Unraveling why we sleep: Quantitative analysis reveals abrupt transition from neural reorganization to repair in early development. *Sci Adv* **6**, (2020).
13. A. B. Nelson, U. Faraguna, J. T. Zoltan, G. Tononi, C. Cirelli, Sleep patterns and homeostatic mechanisms in adolescent mice. *Brain Sci* **3**, 318-343 (2013).
14. A. Suzuki, C. M. Sinton, R. W. Greene, M. Yanagisawa, Behavioral and biochemical dissociation of arousal and homeostatic sleep need influenced by prior wakeful experience in mice. *Proc Natl Acad Sci U S A* **110**, 10288-10293 (2013).
15. A. Suzuki, M. Yanagisawa, R. W. Greene, Loss of Arc attenuates the behavioral and molecular responses for sleep homeostasis in mice. *Proc Natl Acad Sci U S A* **117**, 10547-10553 (2020).
16. S. Maret *et al.*, Homer1a is a core brain molecular correlate of sleep loss. *Proc Natl Acad Sci U S A* **104**, 20090-20095 (2007).
17. W. Li, L. Ma, G. Yang, W. B. Gan, REM sleep selectively prunes and maintains new synapses in development and learning. *Nat Neurosci* **20**, 427-437 (2017).
18. L. Renouard *et al.*, REM sleep promotes bidirectional plasticity in developing visual cortex in vivo. *Neurobiol Sleep Circadian Rhythms* **12**, 100076 (2022).

19. D. D. Wiredja, M. Koyuturk, M. R. Chance, The KSEA App: a web-based tool for kinase activity inference from quantitative phosphoproteomics. *Bioinformatics* **33**, 3489-3491 (2017).
20. K. L. Ode, H. R. Ueda, Phosphorylation Hypothesis of Sleep. *Front Psychol* **11**, 575328 (2020).
21. D. Tone *et al.*, Distinct phosphorylation states of mammalian CaMKIIbeta control the induction and maintenance of sleep. *PLoS Biol* **20**, e3001813 (2022).
22. R. Zhou *et al.*, A signalling pathway for transcriptional regulation of sleep amount in mice. *Nature* **612**, 519-527 (2022).
23. Q. Ye, Q. L. Miao, Experience-dependent development of perineuronal nets and chondroitin sulfate proteoglycan receptors in mouse visual cortex. *Matrix Biol* **32**, 352-363 (2013).
24. T. Pizzorusso *et al.*, Reactivation of ocular dominance plasticity in the adult visual cortex. *Science* **298**, 1248-1251 (2002).
25. H. Takahashi, A. M. Craig, Protein tyrosine phosphatases PTPdelta, PTPsigma, and LAR: presynaptic hubs for synapse organization. *Trends Neurosci* **36**, 522-534 (2013).
26. K. Shen, C. W. Cowan, Guidance molecules in synapse formation and plasticity. *Cold Spring Harb Perspect Biol* **2**, a001842 (2010).
27. M. Makinodan, K. M. Rosen, S. Ito, G. Corfas, A critical period for social experience-dependent oligodendrocyte maturation and myelination. *Science* **337**, 1357-1360 (2012).
28. A. I. Ramsaran *et al.*, A shift in the mechanisms controlling hippocampal engram formation during brain maturation. *Science* **380**, 543-551 (2023).
29. G. H. Diering, R. L. Huganir, The AMPA Receptor Code of Synaptic Plasticity. *Neuron* **100**, 314-329 (2018).
30. R. L. Huganir, R. A. Nicoll, AMPARs and synaptic plasticity: the last 25 years. *Neuron* **80**, 704-717 (2013).
31. H. Y. Zoghbi, Postnatal neurodevelopmental disorders: meeting at the synapse? *Science* **302**, 826-830 (2003).
32. T. Wintler, H. Schoch, M. G. Frank, L. Peixoto, Sleep, brain development, and autism spectrum disorders: Insights from animal models. *J Neurosci Res* **98**, 1137-1149 (2020).
33. K. E. MacDuffie *et al.*, Sleep Onset Problems and Subcortical Development in Infants Later Diagnosed With Autism Spectrum Disorder. *Am J Psychiatry* **177**, 518-525 (2020).
34. G. Missig, C. J. McDougle, W. A. Carlezon, Jr., Sleep as a translationally-relevant endpoint in studies of autism spectrum disorder (ASD). *Neuropsychopharmacology*, (2019).
35. K. E. MacDuffie *et al.*, Sleep Problems and Trajectories of Restricted and Repetitive Behaviors in Children with Neurodevelopmental Disabilities. *J Autism Dev Disord* **50**, 3844-3856 (2020).
36. B. A. Cary, G. G. Turrigiano, Stability of neocortical synapses across sleep and wake states during the critical period in rats. *Elife* **10**, (2021).
37. M. G. Frank, H. C. Heller, The Function(s) of Sleep. *Handb Exp Pharmacol* **253**, 3-34 (2019).
38. A. R. Poe *et al.*, Developmental emergence of sleep rhythms enables long-term memory in Drosophila. *Sci Adv* **9**, eadh2301 (2023).
39. C. M. Muheim *et al.*, Ontogenesis of the molecular response to sleep loss. *Neurobiol Sleep Circadian Rhythms* **14**, 100092 (2023).
40. G. Yang, W. B. Gan, Sleep contributes to dendritic spine formation and elimination in the developing mouse somatosensory cortex. *Dev Neurobiol* **72**, 1391-1398 (2012).

41. Y. Zhou *et al.*, REM sleep promotes experience-dependent dendritic spine elimination in the mouse cortex. *Nat Commun* **11**, 4819 (2020).
42. S. Maret, U. Faraguna, A. B. Nelson, C. Cirelli, G. Tononi, Sleep and waking modulate spine turnover in the adolescent mouse cortex. *Nat Neurosci* **14**, 1418-1420 (2011).
43. L. de Vivo *et al.*, Ultrastructural evidence for synaptic scaling across the wake/sleep cycle. *Science* **355**, 507-510 (2017).
44. J. K. Holth *et al.*, The sleep-wake cycle regulates brain interstitial fluid tau in mice and CSF tau in humans. *Science* **363**, 880-884 (2019).
45. C. Wang, D. M. Holtzman, Bidirectional relationship between sleep and Alzheimer's disease: role of amyloid, tau, and other factors. *Neuropsychopharmacology*, (2019).
46. S. B. Li *et al.*, Hyperexcitable arousal circuits drive sleep instability during aging. *Science* **375**, eabh3021 (2022).
47. K. D. Donohue, D. C. Medonza, E. R. Crane, B. F. O'Hara, Assessment of a non-invasive high-throughput classifier for behaviours associated with sleep and wake in mice. *Biomed Eng Online* **7**, 14 (2008).
48. A. E. Flores *et al.*, Pattern recognition of sleep in rodents using piezoelectric signals generated by gross body movements. *IEEE Trans Biomed Eng* **54**, 225-233 (2007).
49. G. M. Mang *et al.*, Evaluation of a piezoelectric system as an alternative to electroencephalogram/ electromyogram recordings in mouse sleep studies. *Sleep* **37**, 1383-1392 (2014).
50. P. Mertins *et al.*, Reproducible workflow for multiplexed deep-scale proteome and phosphoproteome analysis of tumor tissues by liquid chromatography-mass spectrometry. *Nat Protoc* **13**, 1632-1661 (2018).
51. G. C. McAlister *et al.*, MultiNotch MS3 enables accurate, sensitive, and multiplexed detection of differential expression across cancer cell line proteomes. *Anal Chem* **86**, 7150-7158 (2014).
52. K. Klann *et al.*, Growth Factor Receptor Signaling Inhibition Prevents SARS-CoV-2 Replication. *Mol Cell* **80**, 164-174 e164 (2020).
53. A. Hogrebe *et al.*, Benchmarking common quantification strategies for large-scale phosphoproteomics. *Nat Commun* **9**, 1045 (2018).
54. M. Ashburner *et al.*, Gene ontology: tool for the unification of biology. The Gene Ontology Consortium. *Nat Genet* **25**, 25-29 (2000).
55. C. Gene Ontology *et al.*, The Gene Ontology knowledgebase in 2023. *Genetics* **224**, (2023).
56. P. D. Thomas *et al.*, PANTHER: Making genome-scale phylogenetics accessible to all. *Protein Sci* **31**, 8-22 (2022).
57. S. Poux, P. Gaudet, Best Practices in Manual Annotation with the Gene Ontology. *Methods Mol Biol* **1446**, 41-54 (2017).
58. C. von Mering *et al.*, STRING: known and predicted protein-protein associations, integrated and transferred across organisms. *Nucleic Acids Res* **33**, D433-437 (2005).
59. P. Shannon *et al.*, Cytoscape: a software environment for integrated models of biomolecular interaction networks. *Genome Res* **13**, 2498-2504 (2003).
60. N. T. Doncheva, J. H. Morris, J. Gorodkin, L. J. Jensen, Cytoscape StringApp: Network Analysis and Visualization of Proteomics Data. *J Proteome Res* **18**, 623-632 (2019).
61. P. Casado *et al.*, Kinase-substrate enrichment analysis provides insights into the heterogeneity of signaling pathway activation in leukemia cells. *Sci Signal* **6**, rs6 (2013).
62. P. V. Hornbeck *et al.*, PhosphoSitePlus, 2014: mutations, PTMs and recalibrations. *Nucleic Acids Res* **43**, D512-520 (2015).

63. H. Horn *et al.*, KinomeXplorer: an integrated platform for kinome biology studies. *Nat Methods* **11**, 603-604 (2014).

Acknowledgments: We would like to thank S.K. Monroe for contributing original artwork. We thank Lisa Sharek for technical assistance.

Funding: Simons Foundation Autism Research Initiative #970806 and #385188 (GHD)

This research is based in part upon work conducted using the UNC Proteomics Core Facility, which is supported in part by NCI Center Core Support Grant (2P30CA016086-45) to the UNC Lineberger Comprehensive Cancer Center.

Author contributions:

Conceptualization: GHD, SMG

Methodology: SMG, EC, JSL, SG, TM, MY, NKB, ALM, CAM

Investigation: SMG, EC, JSL, SG, TM, MY

Visualization: GHD, SMG, EC, SG

Funding acquisition: GHD, LEH

Project administration: GHD

Supervision: GHD

Writing – original draft: GHD, SMG

Writing – review & editing: GHD, SMG, LEH

Competing interests: Authors declare that they have no competing interests.

Data and materials availability: All data are available in the main text or the supplementary materials. The mass spectrometry datasets have been deposited in an online data repository PRIDE. Datasets will be made publicly available following peer-reviewed publication.

Supplementary Materials

Materials and Methods

Figs. S1 to S#1-5

Supplementary references (47-63)

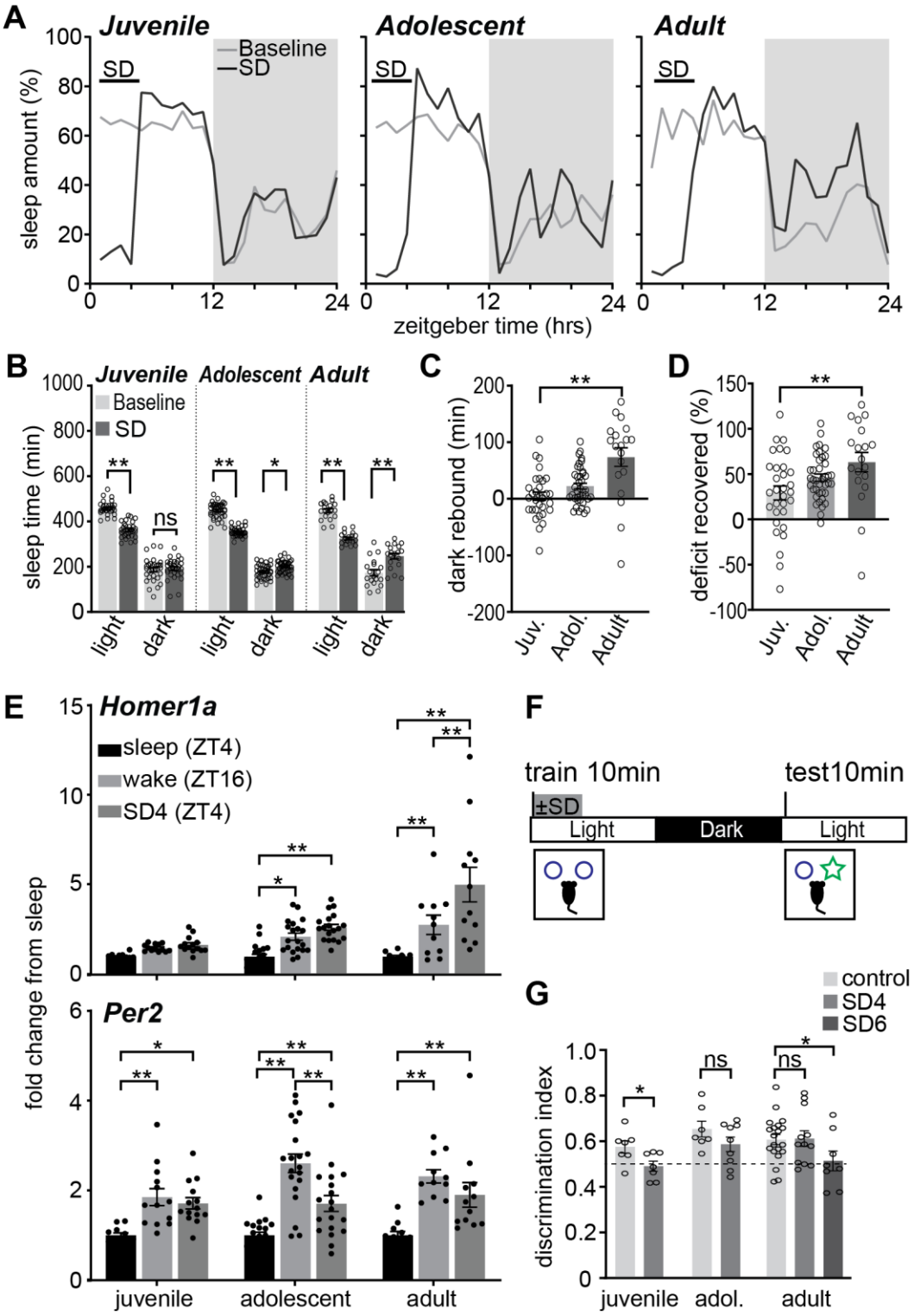

Fig. 1. Lack of robust homeostatic adaptations confers heightened vulnerability to SD in juveniles. (**A**) 24hr sleep trace during uninterrupted baseline or during 4hr SD treatment (ZT0-4) and subsequent recovery (ZT4-24) from juvenile (P28), adolescent (P42), or adult mice (P100). Shaded box indicates dark phase. (**B**) Total sleep time in the light and dark phase during baseline or SD+recovery. Significant dark phase sleep rebound is measured in adolescents and adults, but

not juveniles. *P<0.05, **P<0.01, ns: not significant, 2-way ANOVA, Sidak's correction. (**C and D**) comparison of dark phase sleep rebound and sleep deficit recovery between ages. Rebound measured as increased dark phase sleep amount during SD+recovery over baseline. Deficit calculated based on sleep lost compared to baseline during SD treatment ZT0-4; recovery calculated from increased sleep over baseline from ZT4-24. Dark phase sleep rebound, and sleep deficit recovered, is significantly greater in adults than juveniles. **P<0.01, 1-way ANOVA, Tukey's correction. (**E**) Homer1a and Per2 transcripts measured using qPCR in whole forebrain from juvenile (P21), adolescent (P42), or adult mice (P100). Samples collected during the sleep phase (ZT4), wake phase (ZT16), or immediately following SD4 (ZT4). *P<0.05, **P<0.01, 1-way ANOVA, Tukey's correction. (**F and G**) Juvenile (P28), adolescent (P42), or adult mice (P100) subjected to the novel object recognition task ±SD. Training occurs ZT0-1 followed by uninterrupted control or 4-6hr SD treatment, testing occurs 24hrs after training. Novel object memory performance is completely impaired by SD4 in juveniles, memory impaired by SD6 in adults. *P<0.05, ns: not significant, Student's t-test. Data includes both sexes. Error bars, mean ±SEM.

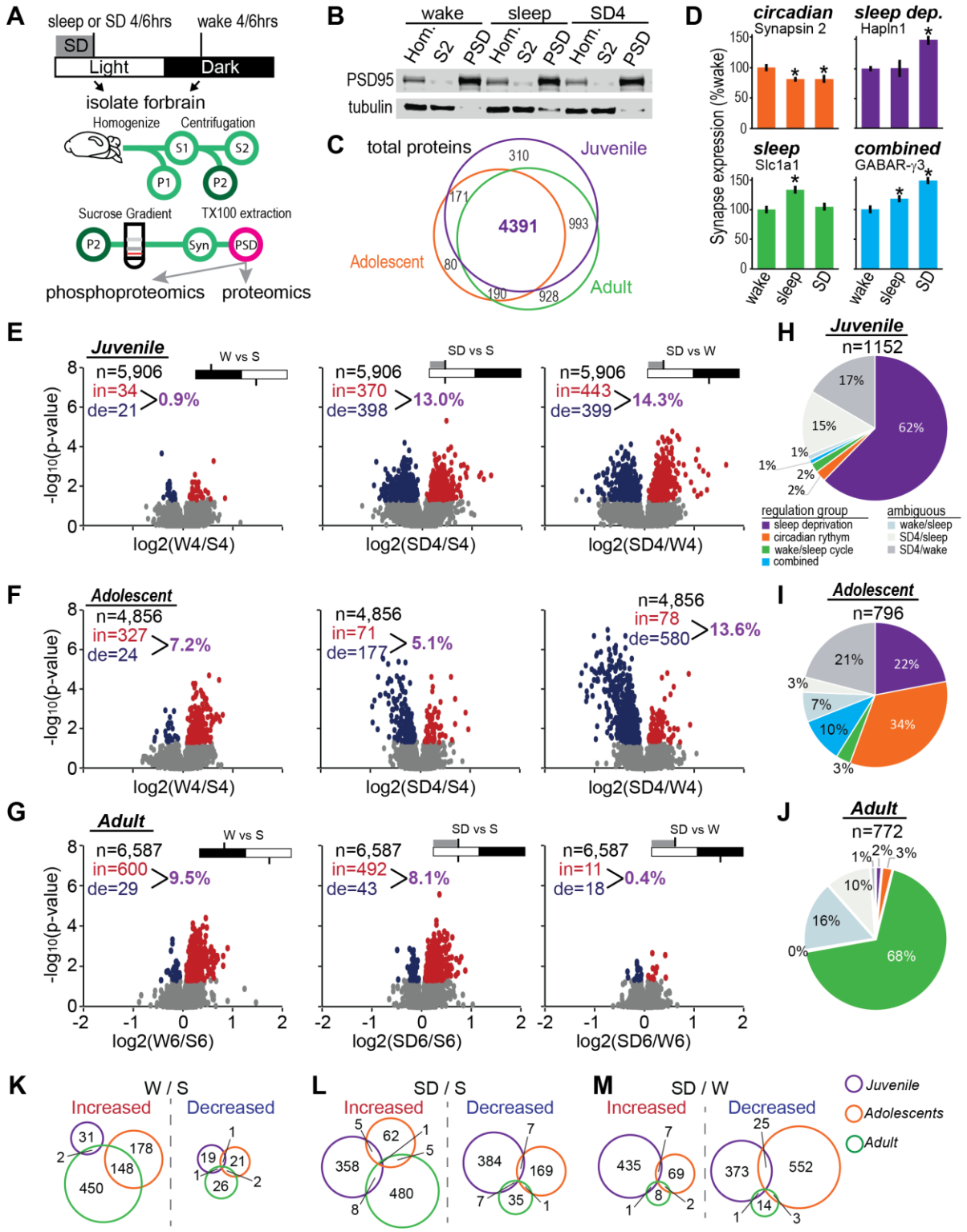

Fig. 2. The juvenile synapse proteome is highly vulnerable to SD, transitions to wake/sleep regulation in adults. (**A**) Experimental design. Isolated forebrain synapse fractions (PSD) from juvenile (P21), adolescent (P42), or adult mice (P100) analyzed by quantitative mass

spectrometry. 4 mice pooled per sample; samples prepared in quadruplicate. Juveniles and adolescents: W4/S4/SD4; adults W6/S6/SD6 conditions (**B**) Representative western blot from juvenile cohorts demonstrating enrichment of synapse scaffold protein PSD95 in the PSD fraction from wake, sleep, or SD conditions. (**C**) Venn diagram depicts high overlap in the proteins detected in the synapse fractions from juveniles, adolescents or adults. (**D**) Examples of juvenile synapse proteins regulated by circadian rhythm (circadian), wake/sleep cycle (sleep), selective response to SD (sleep dep.) or combined. *P<0.05, Student's *t* test with Bonferroni correction. (**E-G**) volcano plots showing changes in synapse proteins in wake/sleep, SD/sleep, and SD/wake comparisons from juvenile, adolescent, or adult mice. N: number of proteins quantified; in and de: proteins significantly increased or decreased respectively (p<0.05, Student's *t* test). Total percentage of proteome altered in each comparison is indicated. (**H-J**) pie charts indicate the significantly altered proteins assigned to regulation groups. Juvenile regulated proteins dominated by selective SD response, adults dominated by regulation from the wake/sleep cycle. (**K-M**) Venn diagrams depict overlap between ages in proteins significantly increased or decreased in each of the pairwise comparisons. Minimal overlap between ages in significantly regulated proteins under all conditions examined, with the exception of proteins upregulated in the wake/sleep comparison that showed substantial overlap between adolescents and adults.

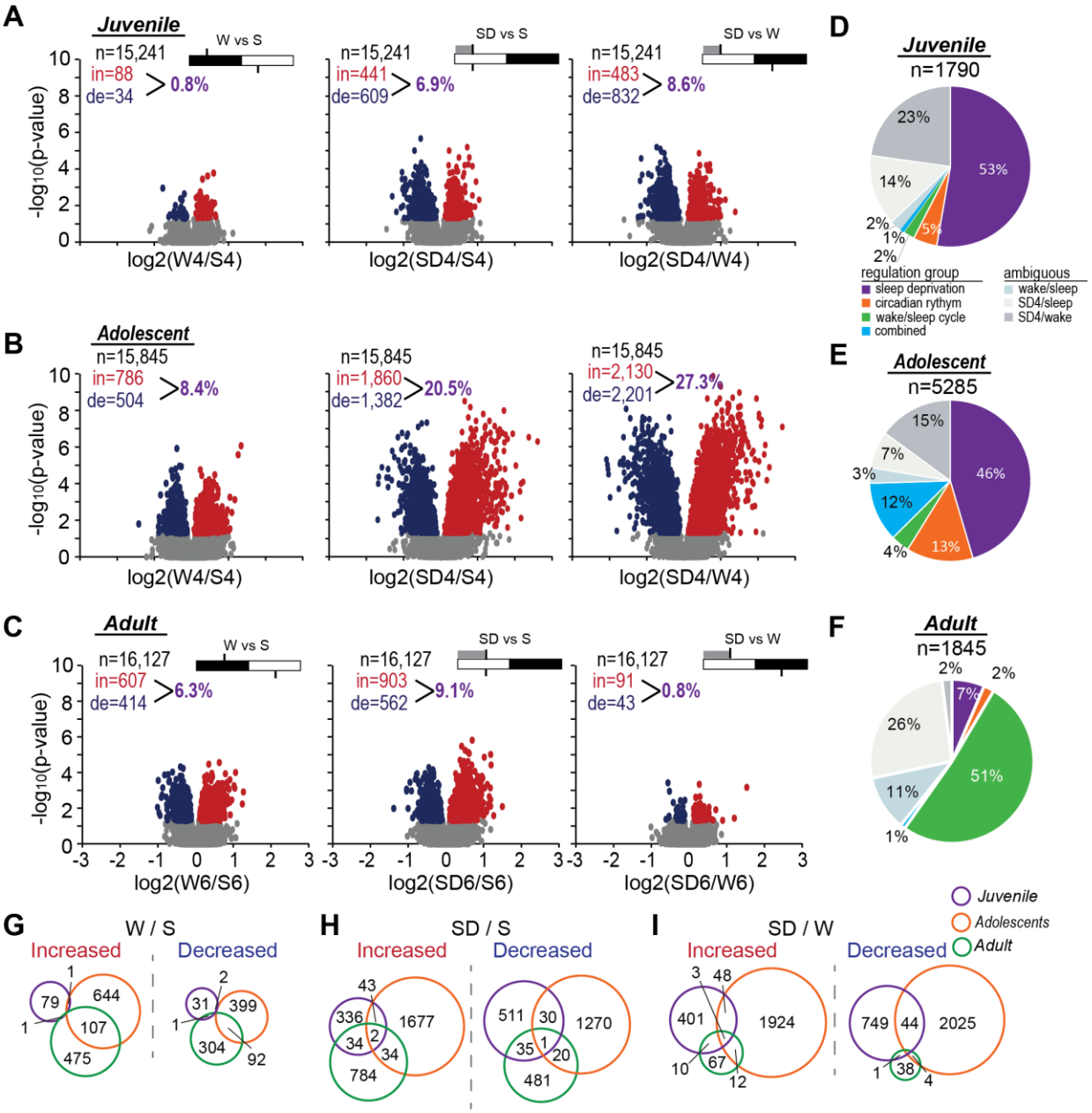

Fig. 3. The developing synapse phosphoproteome is highly vulnerable to SD. (**A-C**) volcano plots showing changes in synapse phosphopeptides in wake/sleep, SD/sleep, and SD/wake comparisons from juvenile, adolescent, or adult mice. N: number of phosphopeptides quantified; in and de: phosphopeptides significantly ($p<0.05$, Student's *t* test) increased or decreased respectively. Total percentage of phosphoproteome altered in each comparison is indicated. (**D-F**) pie charts indicate the significantly altered phosphopeptides assigned to regulation groups. Juvenile and adolescent regulated phosphopeptides dominated by selective SD response, adults dominated by regulation from the wake/sleep cycle. (**G-I**) Venn diagrams depict overlap between ages in phosphopeptides significantly increased or decreased in each of the pairwise comparisons. Minimal overlap between ages under all conditions examined.

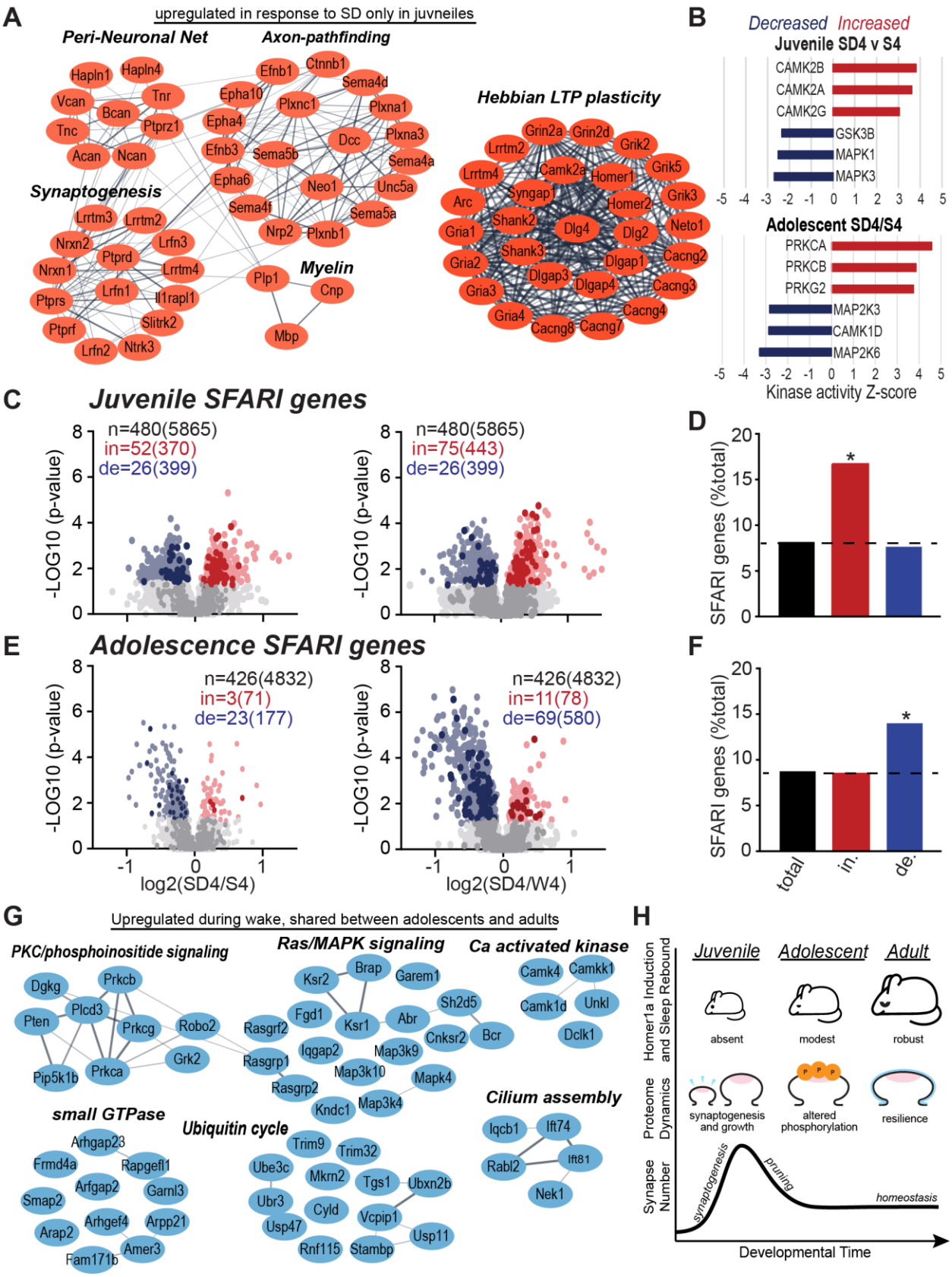
A
upregulated in response to SD only in juvneiles
Peri-Neuronal Net
Axon-pathfinding
Synaptogenesis
Myelin
Hebbian LTP plasticity
B
Decreased
Increased
Juvenile SD4 v S4
CAMK2B
CAMK2A
CAMK2G
GSK3B
MAPK1
MAPK3
Adolescent SD4/S4
PRKCA
PRKCB
PRKG2
MAP2K3
CAMK1D
MAP2K6
Kinase activity Z-score
C
Juvenile SFARI genes
n=480(5865)
in=52(370)
de=26(399)
n=480(5865)
in=75(443)
de=26(399)
-LOG10 (p-value)
D
SFARI genes (%total)
E
Adolescence SFARI genes
n=426(4832)
in=3(71)
de=23(177)
n=426(4832)
in=11(78)
de=69(580)
log2(SD4/S4)
log2(SD4/W4)
F
total
in.
de.
G
Upregulated during wake, shared between adolescents and adults
PKC/phosphoinositide signaling
Ras/MAPK signaling
Ca activated kinase
small GTPase
Ubiquitin cycle
Cilium assembly
H
Juvenile
Adolescent
Adult
Homer1a Induction and Sleep Rebound
absent
modest
robust
Proteome Dynamics
synaptogenesis and growth
altered phosphorylation
resilience
Synapse Number
synaptogenesis
pruning
homeostasis
Developmental Time

Fig. 4. Distinct synaptic responses indicate unique roles of sleep in supporting brain development. (**A**) Synapse proteins upregulated in response to SD only in juveniles, related to brain development and synapse potentiation. Protein interaction network identified using gene ontology (GO) and STRING analysis. (**B**) KSEA indicates SD drives activation of CaMKII isoforms in juveniles and classic PKC isoforms in adolescents, (**C-F**) volcano plots: SD induced changes in SFARI risk genes (bold color). Number of SFARI genes detected (n), increased (in) or decreased (de) compared to total are indicated. Bar charts: * indicates SD response is significantly enriched for SFARI genes compared to expected overlap from total (dashed line; hyper geometric test). Juvenile (C and D); Adolescents (E and F). (**G**) Protein interaction network depicting proteins upregulated in wake/sleep comparisons common to both adolescents and adults. (**H**) Schematic summary model. Sleep and SD exert distinct effects during periods of active synapse maturation: synaptogenesis and pruning, compared to periods where synapse densities stabilize during transition to adulthood.

Supplementary material
Materials and Methods
Mice

All animal procedures were approved by the Institutional Animal Care and Use Committee of the University of North Carolina (UNC) at Chapel Hill and were performed in accordance with the guidelines of the U.S. National Institutes of Health. All experiments were performed using C57Bl/6J mice of both sexes purchased from Jackson Labs, or bred in house. Adult mice for all experiments were purchased from Jackson Labs and acclimated to UNC housing for at least 2 weeks prior to the start of the experiment. For experiments using juvenile or adolescent mice, experimental animals were bred in house with adult breeders purchased from Jackson Labs. Breeders for our colony were replaced every 3 months with mice supplied from Jackson Labs. Target experimental ages for adolescents was P42 and adults P90. For juveniles, target age for biochemistry experiments was P21, target age for behavior studies was P28. Specific age ranges are stated below for each experiment.

Sleep recordings and calculations

Sleep-wake behavior of juvenile (postnatal day, p25-35), adolescent (p41-45), and adult (p70-100) C57BL/6J mice was recorded continuously using a non-invasive piezoelectric monitoring system (PiezoSleep 2.0; Signal Solution, LLC, Lexington, KY). Separate cohorts were generated for each of the age groups. First, mice were transferred to our satellite facility, maintained on a 12hr:12hr light:dark cycle. Mice were housed individually (15.5 cm^2 cages) and provided with bedding, water, and food. Following a 36-48hr acclimation period, sleep and wake behavior was recorded for at least 24 hours to establish a baseline. Next, mice were subjected to a 4hr gentle handling sleep deprivation (SD4) at the onset of the light cycle (zeitgeber time, ZT0-4) and allowed to recover for the remainder of the day (ZT4 – ZT24), wakefulness assessed by continued observation from experimenters as described previously (*14*).

The PiezoSleep monitoring system utilizes a piezoelectric mat positioned underneath the mouse cage to detect vibrational movements, such as breathing. A customized statistics software (SleepStats, Signal Solution, Lexington, KY) processes these signals through an algorithm, distinguishing distinct respiratory patterns associated with sleep and wake states. Sleep is typified by periodic (2-3 Hz), regular amplitude signal, a common respiratory feature during mouse sleep states. In contrast, wakefulness is identified by the absence of standard sleep signals and the presence of irregular, higher amplitude signals, typically observed during voluntary movement (including subtle movements seen in quite wake). Using a linear discriminant classifier algorithm, the piezoelectric signals were classified as “sleep” or “wake” in 2-second epochs. Sleep-wake thresholds were automatically calculated for each individual mouse. To exclude brief or ambiguous arousals, a sleep bout is initiated when a 30 sec epoch contains greater than 50% sleep and is terminated when a 30 sec epoch contains less than 50% sleep. Validation of this software has been conducted using a combination of electroencephalography, electromyography, and visual assessment (*47-49*).

Sleep amount generated through the SleepStats software was analyzed to characterize sleep-wake patterns on the day of sleep deprivation (SD) and the day prior (Baseline). Sleep amount data was binned into 1hr intervals to generate daily sleep traces and calculate average sleep amount during the light and dark cycles. Dark phase sleep rebound was calculated by subtracting baseline dark cycle sleep from dark cycle sleep on the day of sleep deprivation for each individual mouse. Deficit recovered was determined in three steps. First the average amount of sleep loss during SD4 was calculated for each age group. Second, total sleep rebound was calculated by subtracting the amount of sleep between ZT4-ZT24 at baseline from the amount of

sleep in the period following SD4 (ZT4-ZT24). Finally, the deficit recovered was determined by dividing the total sleep rebound by the average sleep loss, calculated as a percent ($\frac{Total\ sleep\ rebound}{Average\ sleep\ loss} x\ 100 = \%\ deficit\ recovered$). A 2-way ANOVA followed by a Sidak's multiple comparisons test was used to analyze total sleep time. The dark rebound and percent deficit recovered were analyzed with a one-way ANOVA followed by a Tukey's multiple comparisons test.

Quantitative Real-Time PCR

Forebrain (cortex and hippocampus) were dissected from juvenile (P21-22), adolescent (P42-46), and adult (P90) mice. (mRNA was purified using the RNeasy Plus Mini Kit (Qiagen 74136) according to the manufacturer's instruction. RNA was reverse transcribed into cDNA using the High-Capacity cDNA Reverse Transcription Kit (Applied Biosystems 4374966). Quantitative real-time PCR (RT-qPCR) was performed using the QuantStudio 7 Flex (Applied Biosystems) using Taqman Fast Advanced Master Mix (Applied Biosystems 4444557) and Taqman primer/probes for GAPDH (Invitrogen, Mm99999915_g1), Per2 (Invitrogen, Mm00478099) and Homer1a (Invitrogen custom Taqman Assay, APNKUGG). Expression data were calculated as fold gene expression using $2^{-\Delta\Delta Ct}$ method with GAPDH as the reference gene and normalized to the sleep (ZT4) condition. Four independent technical replicates were performed in each individual experiment. The resulting data was analyzed with a 2-way ANOVA followed by Tukey's multiple comparisons test.

Novel Object Recognition (NOR) assay and analysis

Mice were tested at one of three age points: juvenile (P28); adolescent (P42); and adult (P100). All experimental manipulations took place in a lab-maintained behavior assay room ("behavior room"). The experimental apparatus was composed of four open-topped cubes arranged in a quadrant formation at table height. The cubes were 40cm3 and were lined with napped gray Kydex. One wall in each cage had a visual cue so that animals could spatially orient themselves. Small action cameras (AKASO EK7000 Pro) were positioned directly over each chamber to record the mice during the experiment. Each chamber also had a dedicated light source directly overhead to allow for dim lighting conditions, with the overhead lights off, during the NOR testing. The objects were pairs of identical glass salt shakers or similarly sized black plastic canisters. The objects were weighted to prevent tipping or sliding, and they were positioned within each cage using a measured placement guide. Chambers and objects were cleaned with ethanol between subjects, and subjects were returned to the same chamber for training and testing.

For three days prior to training, all mice were lightly handled for 10 minutes to acclimatize the mice to the experimenters. By the third day, all animals could perch calmly in the experimenter's palm without voiding or trying to escape.

On training day, all subjects in a cohort were brought to the behavior room in their home cages at ZT1. Each mouse freely explored one chamber with two identical objects in fixed locations for 10 minutes. Four animals were trained simultaneously. After 10 minutes, mice were returned to their home cages with their cage mates and either allowed to have undisturbed sleep (control) or gentle handling sleep deprivation for 4 hours (SD4) or 6 hours (SD6). Sleep deprivation took place in the home cage in the behavior room.

On testing day, the following morning, all subjects were brought back to the behavior room in their home cages at ZT2. Each mouse was returned to its training cage and allowed to freely explore for 10 minutes one familiar training object and one novel object (whichever class

of object was not used for that mouse's training) in the same fixed locations as during training. Four animals were again tested simultaneously. The experiment was concluded once each mouse completed its testing exposure, and the chambers and objects were deep cleaned and sanitized.
Scoring: A scoring function was developed in-house using Oracle OpenJDK Version 17.0.1. It was used in the IntelliJ IDEA 2021.3.1 IDE by scorers to record beginning and end points, in milliseconds, of an interaction with each object, while viewing the video recording of the testing sessions. The scorers were blind to mouse sleep condition and familiar/novel object status during the time of scoring. The function also recorded all beginning points of interactions ("Time stamps"), as well as the beginning and end time points of the scoring process/video.

Interactions were defined as any continuous period during which the mouse was within one head-length from the object of interest and looking directly at the object. If the mouse looked away or climbed on top of the object, the interaction period ended.
Data analysis: Values for total time spent interacting with each object (Total Interaction Time) and total novel object interaction time divided by total overall object interaction time (Discrimination Index) were calculated and subsequently exported to GraphPad Prism 9.5.1 for figure development and statistical analyses. Statistical values for Total Interaction Time were calculated using paired t-tests, comparing within-mouse novel object and familiar object interaction time values. Statistical values for Discrimination Index were calculated using unpaired t-tests comparing control and sleep-deprived mice within each age group.

PSD preparation

Developing (juvenile, P21-22 and adolescent mice, P42-46) mice were sacked at ZT4 (sleep), ZT16 (wake), or at ZT4 following SD4. Adult mice (P90-110) were sacrificed undisturbed at ZT4/ZT16 or immediately following SD4 (ZT4), or undisturbed at ZT6 (sleep), ZT18 (wake), or immediately following SD6 (ZT6). An equal amount of male and females were used for each condition and age, allowing us to determine changes independent of sex. Once sacked, the forebrain was dissected and immediately flash frozen.

Frozen forebrains were homogenized using 15 strokes from an ice-cold homogenizer in ice cold homogenization solution (320mM sucrose, 10mM HEPES pH 7.4, 1mM EDTA, 5mM Na pyrophosphate, 1mM Na_3VO_4, 200nM okadaic acid, protease inhibitor cocktail). The brain homogenate was then spun at 1,000xg for 10min at 4°C to obtain the P1 (nuclear) and S1 (post-nuclear) fractions. The S1 fraction was layered on top of a discontinuous sucrose density gradient (0.8M, 1.0M or 1.2M sucrose in 10mM HEPES pH 7.4, 1mM EDTA, 5mM Na pyrophosphate, 1mM Na3VO4, 200nM okadaic acid, protease inhibitor cocktail) and subjected to ultra-centrifugation at 82,500xg for 1.5hr at 4°C. The brain material present at the interface of the 1.0M and 1.2M sucrose buffers (synaptosomes) was collected. Synaptosomes were diluted using 10mM HEPES pH7.4 (containing protease and phosphatase inhibitors) to 320mM sucrose concentration. The diluted synaptosomes were pelleted by centrifugation at 100,000xg at 4°C for 20min. The pellet was resuspended in 50mM HEPES pH 7.4 and then mixed with an equal part 1% Triton X-100 (both solutions contained protease and phosphatase inhibitors). The mixture was incubated at 4°C for 15 minutes before being pelleted by centrifugation at 32,000xg for 20min at 4°C to yield the post-synaptic density (PSD) fraction. The pellet was then resuspended in 50mM pH 7.4 (plus protease and phosphatase inhibitors). The protein concentration was determined using Bradford assay. For proteomics and phophosproteomics 4 mice were pooled together for each individual sample analyzed.

Proteomics and Phosphoproteomic preparation and analysis

A total of four sample sets (juvenile, adolescent, adult SD4, adult SD6) were processed for proteomics and phosphoproteomics analysis. PSD lysates (0.5 mg per sample) were reduced with 5mM DTT for 45 min at 37ºC, alkylated with 15mM iodoacetamide for 30 min in the dark at room temperature, then diluted to 1M urea with 50mM ammonium bicarbonate (pH 7.8). Samples were digested with LysC (Wako, 1:50 w/w) for 2 hr at 37ºC, then digested with trypsin (Promega, 1:50 w/w) overnight at 37ºC. The resulting peptide samples were acidified, desalted using desalting spin columns (Thermo), then the eluates were dried via vacuum centrifugation. Peptide concentration was determined using Quantitative Colorimetric Peptide Assay (Pierce).

Twelve total samples and four pooled samples per experiment were labeled with TMTpro (Thermo Fisher) for 1 hr at room temperature. Prior to quenching, the labeling efficiency was evaluated by LC-MS/MS analysis. After confirming >98% labeling efficiency, samples were quenched with 50% hydroxylamine to a final concentration of 0.4%. Labeled peptide samples were combined 1:1, desalted using Thermo desalting spin column, and dried via vacuum centrifugation. The dried TMT-labeled samples (four different set in total) were fractionated using high pH reversed phase HPLC (*50*). Briefly, the samples were offline fractionated over a 90 min run, into 96 fractions by high pH reverse-phase HPLC (Agilent 1260) using an Agilent Zorbax 300 Extend-C18 column (3.5-µm, 4.6 × 250 mm) with mobile phase A containing 4.5 mM ammonium formate (pH 10) in 2% (vol/vol) LC-MS grade acetonitrile, and mobile phase B containing 4.5 mM ammonium formate (pH 10) in 90% (vol/vol) LC-MS grade acetonitrile. The 96 resulting fractions were then concatenated in a non-continuous manner into 24 fractions and 5% of each were aliquoted, dried down via vacuum centrifugation and stored at -80ºC until further analysis.

The remaining 95% of each fraction was further concatenated into 6 fractions and dried down via vacuum centrifugation. For each fraction, phosphopeptides were enriched using the High Select Fe-NTA kit (Thermo) per manufacturer protocol, then the Fe-NTA eluates were dried down via vacuum centrifugation and stored at -80ºC until further analysis.

<u>LC/MS/MS Analysis:</u> Each experiment consisting of 24 fractions for the proteome analysis and 6 fractions for the phosphoproteome analysis were analyzed by LC/MS/MS using an Easy nLC 1200-Orbitrap Fusion Lumos Tribrid or an Ultimate 3000-Exploris480 (Thermo Scientific). On the Lumos platform, samples were injected onto an Easy Spray PepMap C18 column (75 µm id × 25 cm, 2 µm particle size) (Thermo Scientific) and separated over a 120 min method. The gradient for separation consisted of 5–42% mobile phase B at a 250 nl/min flow rate, where mobile phase A was 0.1% formic acid in water and mobile phase B consisted of 0.1% formic acid in 80% acetonitrile.

For the proteome fractions, the Lumos was operated in SPS-MS3 mode (*51*), with a 3s cycle time. Resolution for the precursor scan (m/z 400–1500) was set to 120,000 with a AGC target set to standard and a maximum injection time of 50 ms. MS2 scans consisted of CID normalized collision energy (NCE) 32; AGC target set to standard; maximum injection time of 50 ms; isolation window of 0.7 Da. Following MS2 acquisition, MS3 spectra were collected in SPS mode (10 scans per outcome); HCD set to 55; resolution set to 50,000; scan range set to 100-500; AGC target set to 200% with a 100 ms maximum inject time. For the phosphoproteome fractions, which were analyzed in duplicate, the Lumos was operated in MS2 mode (*52, 53*) with a 3s cycle time. Resolution for the precursor scan (m/z 400–1500) was set to 60,000 with a AGC target set to standard and a maximum injection time of 50 ms. For MS2 scans, HCD was set to 35; AGC target set to 200%; maximum injection time of 120 ms; isolation window of 0.7 Da; resolution set to 50,000.

On the Exploris platform, the proteome and phosphoproteome fractions were analyzed using a turboTMT method (*51*). Samples were injected onto an Ion Opticks Aurora C18 column (75 µm id × 15 cm, 1.6 µm particle size) and separated over a 70 or 100 min method. The gradient for separation consisted of 5–42% mobile phase B at a 250 nl/min flow rate, where mobile phase A was 0.1% formic acid in water and mobile phase B consisted of 0.1% formic acid in 80% ACN. The Exploris480 was operated in turboTMTpro mode with a cycle time of 3s. Resolution for the precursor scan (m/z 375–1400) was set to 60,000 with a AGC target set to standard and a maximum injection time set to auto. MS2 scans (30,000 resolution) consisted of higher collision dissociate (HCD) set to 38; AGC target set to 300%; maximum injection time set to auto; isolation window of 0.7 Da; fixed first mass of 110 m/z.

Data Analysis: Raw data files were processed using Proteome Discoverer version 2.5, set to 'reporter ion MS2' or 'reporter ion MS3' with '16pex TMT'. Peak lists were searched against a reviewed Uniprot mouse database (downloaded Feb 2021 containing 17,051 sequences), appended with a common contaminants database, using Sequest HT within Proteome Discoverer. Data were searched with up to two missed trypsin cleavage sites, fixed modifications: TMT16plex peptide N-terminus and Lys, carbamidomethylation Cys, dynamic modification: N-terminal protein acetyl, oxidation Met. For phosphoproteome data, additional dynamic modification: phosphorylation Ser, Thr, Tyr. Precursor mass tolerance of 10ppm and fragment mass tolerance of 0.02 Da (MS2) or 0.5 Da (MS3). Peptide false discovery rate was set to 1%. Reporter abundance was calculated based on intensity, and for MS2 data, co-isolation threshold was set to 50; for MS3 data, SPS mass matches threshold was set to 50 and co-isolation threshold was set to 100. For proteome data, razor and unique peptides were used for quantitation. Proteins and phosphopeptides with >50% missing TMT intensities across samples were removed. Student's t-tests were conducted within Proteome Discoverer, and a p-value <0.05 was considered significant. Log2 fold change ratios were calculated for each pairwise comparison. For the proteomic data set, proteins with PSM = 1 & only one unique peptidewere removed. Proteins identified as contaminants were removed. For the phosphoproteomic dataset, only phosphopeptides identified every sample for a given age group were analyzed.

Bioinformatics and analysis

For analysis, visualization, and bioinformatics, significantly changing proteins and phosphoproteins used were pulled from one of three subsets. The first subset are the significantly changing proteins/ phosphopeptides (p<0.05) from individual comparisons i.e. SD4 v ZT4, SD4 v ZT16, or ZT16 v ZT4, called regulated synapse proteins/phosphopeptides. The second subset are proteins assigned to regulation groups based on significantly changing in one comparison (p<0.05) and (p<0.1) in at least one other comparison. The proteins and phosphopeptides were then designated a regulation group i.e. sleep deprivation, circadian rhythm, etc, based on these cut offs. This statistical cut off allows us to describe more broadly strong overall data trends, and was used to generate pie charts depicted in Figure 2 and 3. The third subset were the high confidence regulation groups. For this subset, proteins/phosphopeptides were designated a regulation group based on a significance cut off of p<0.05 for 2 or more comparisons. This comparison was used in the SFARI data base comparison

GO term and STRING analysis: To determine relevant biological and mechanistic pathways effected by sleep or sleep deprivation both the Gene Ontology data base and STRING analysis were used in conjunction with literature review. High confidence significantly changing protein gene names were input into the Gene Ontology (GO) database (*54, 55*). The GO database utilizes

the PANTHER data base classification system to indicate groups of proteins that are represented significantly more than expected and identifies the associated GO terms (*56*). A false discovery rate (FDR) of 0.05 was the cut off for determining GO terms. GO terms were prioritized based on FDR, the PANTHER data base classification of GO term families, and with manual curation, using GO term curation guidelines (*57*). STRING analysis was performed on high confidence significantly changing proteins (*58*) on Cytoscape (*59, 60*). A confidence score of 0.4 with no maximum interactors were used as cut offs. Apparent clusters were chosen and identified with GO term analysis and manual identification.

KSEA: Kinase-Substrate Enrichment Analysis (KSEA) was used to determine the predicted kinase activity from the phosphoprotoemic data set (*61-63*). The significantly changing phosphopeptides for each comparison were input in to the KSEA app software (4). Both the PhosphoSitePlus and NetworKIN databases were used. A score cutoff of 2 was used for the NetworKIN results. The kinases shown were predicted to significantly change in activity ($p<0.05$) and have 3 or more substrates.

Supplementary Figures

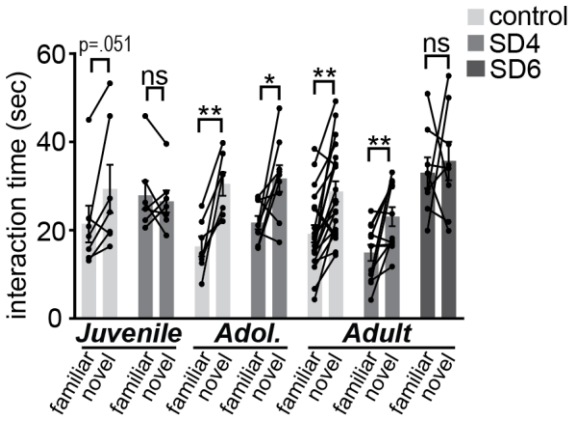

Fig. S1. NOR object interaction time. Interaction time with familiar and novel objects in the novel object recognition task. *P<0.05, **P<0.01, ns: not significant, paired Student's t-test.

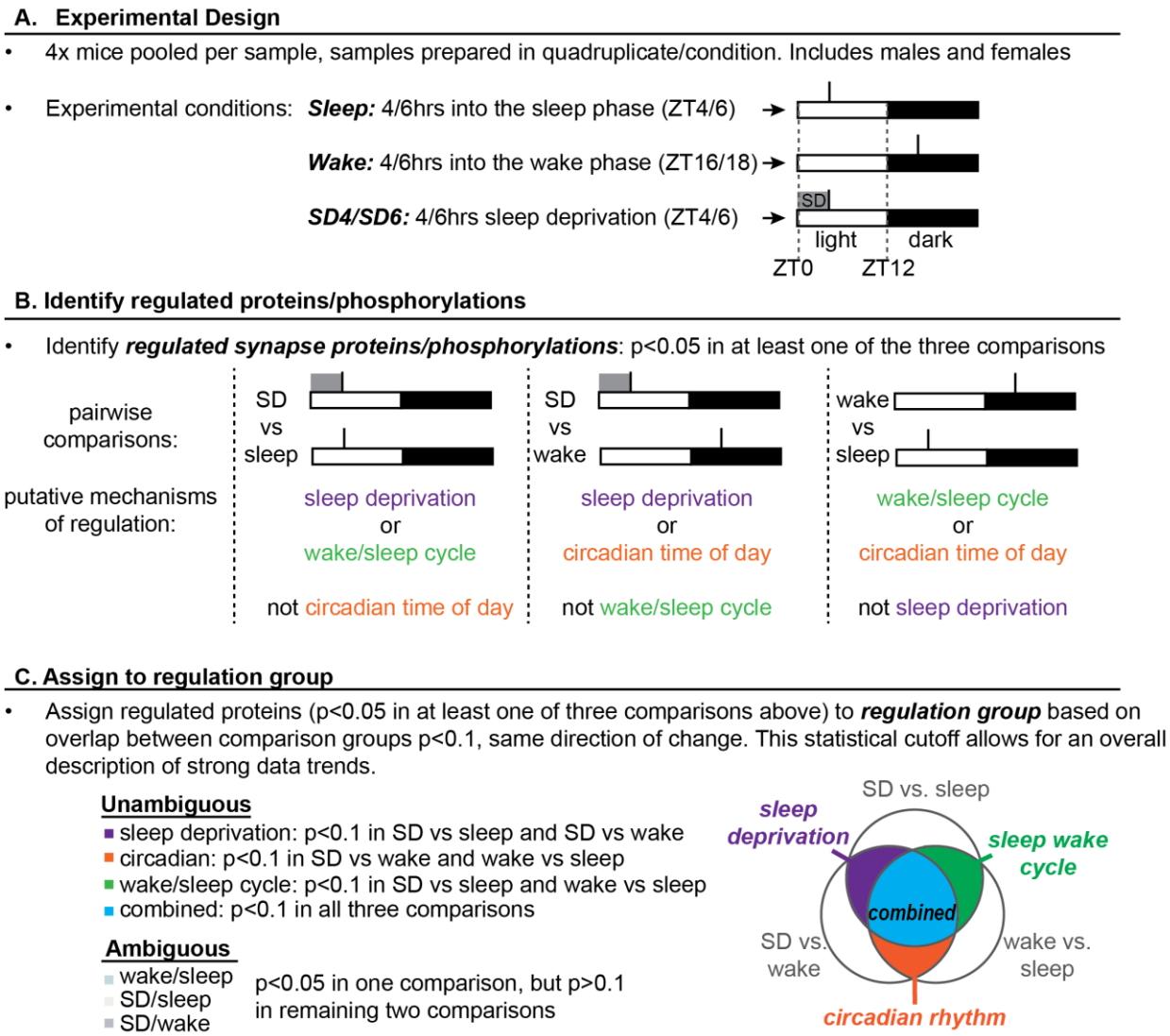

Fig. S2. Interpretation of significantly regulated proteins and phosphopeptides. (**A**) experimental design. Mouse forebrain samples collected during wake or sleep phases, or following SD, 4 mice pooled per sample, samples prepared in quadruplicate. (**B**) pairwise comparisons between conditions identifies significantly regulated proteins. (**C**) regulated proteins assigned to regulation groups.

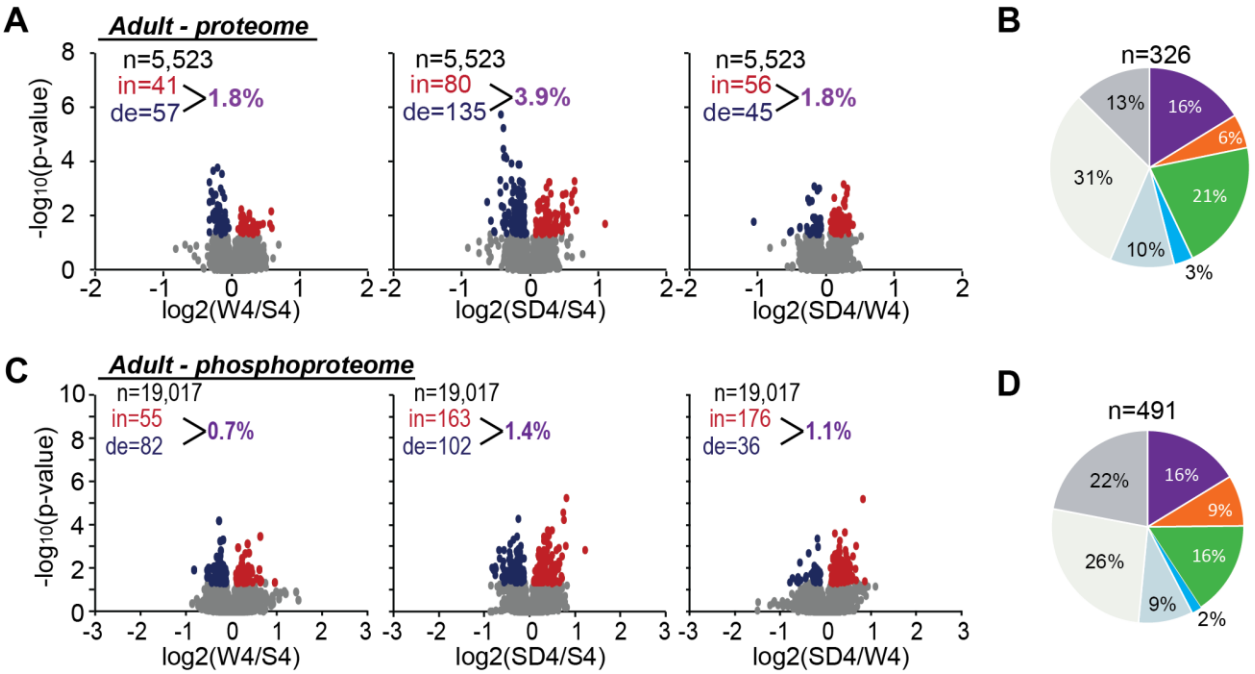

Fig. S3. SD4 effects on adult synapse proteome and phosphoproteome. (**A**) volcano plots showing changes in synapse proteins in W4/S4, SD4/S4, and SD4/W4 comparisons from adult mice. N: number of proteins quantified; in and de: proteins significantly ($p<0.05$, Student's *t* test) increased or decreased respectively. Total percentage of proteome altered in each comparison is indicated. (**B**) pie charts indicate the significantly altered proteins assigned to regulation groups. (**C and D**) Volcano plots and pie charts of adult phosphoproteome from W4/S4/SD4 conditions.

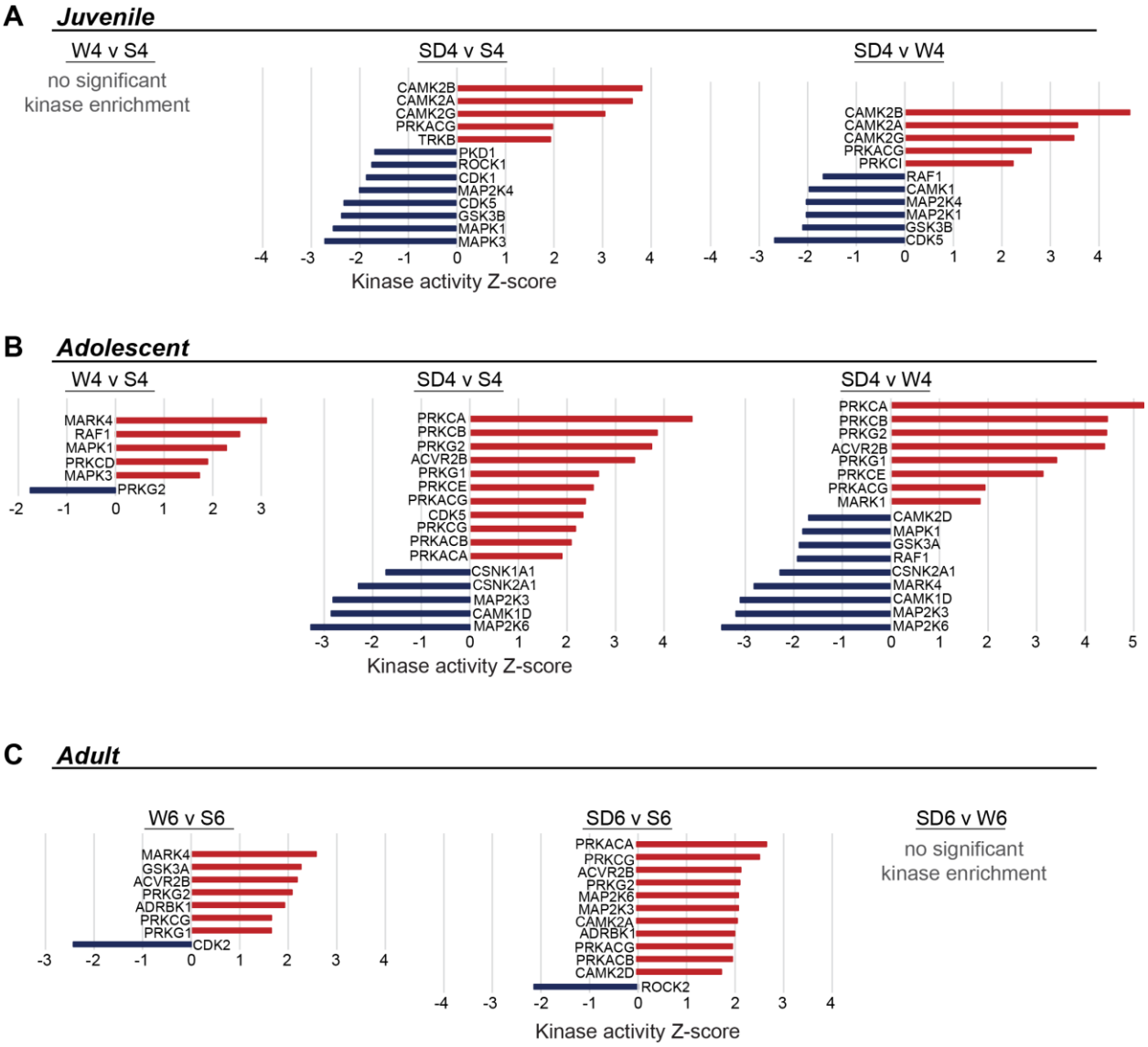

Fig. S4. Kinase activity predictions from developing and adult synapse phosphoproteome. (**A-C**) Kinase substrate enrichment analysis (KSEA) was used to predict upregulated (red) or downregulated (blue) kinase activity in WvS, SDvS, and SDvW comparisons from each age.

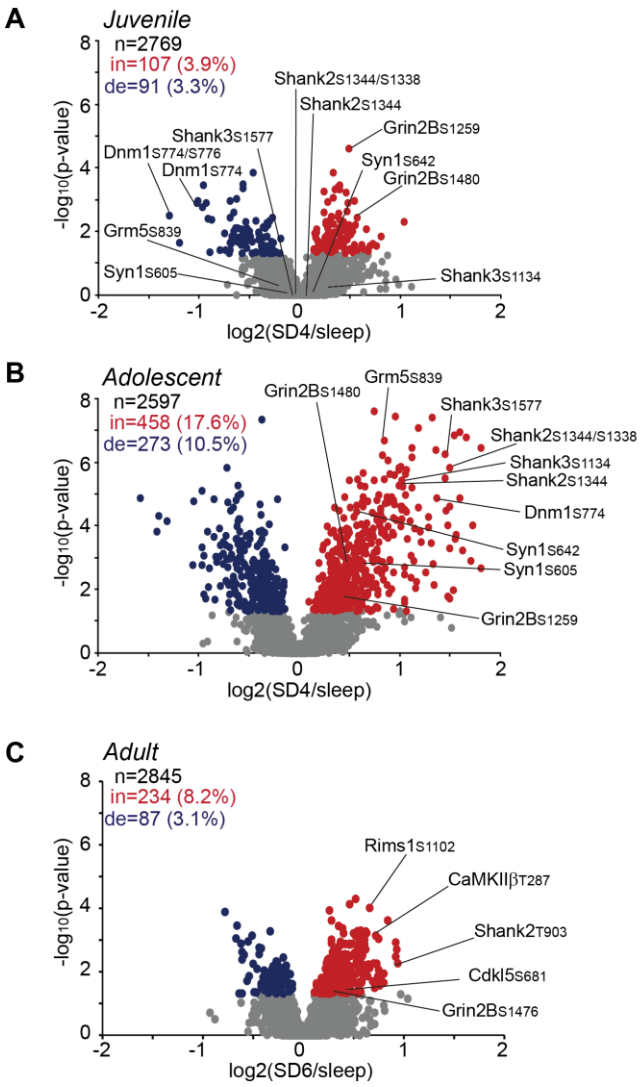

Fig. S5. Analysis of previously identified sleep need index phosphoproteins (SNIPPs). (**A-C**) Volcano plots depicting phosphopeptides quantified from previously identified sleep need index phosphoproteins (SNIPPs) from juveniles (A), adolescents (B), and adults (C). SNIPPs display an asymmetric increase in adolescents and adults as previously described, whereas juveniles display a largely symmetric response with similar numbers of SNIPP phosphorylations increased and decreased.